EPJ Web of Conferences **356**, 02027 (2026) https://doi.org/10.1051/epjconf/202635602027
ICC 2025

In Silico Engineering of Plant-Derived Biomolecules: Predicting Efficacy Parameters for Medicinal Applications

Akhilesh Kumar Gupta[1], Shardul Vadalkar[1, 2], Keyur N. Vyas[1] and Prafulla K. Jha[1,],*

[1]Department of Physics, Faculty of Science, The Maharaja Sayajirao University of Baroda, Vadodara, Gujarat – 390002, India
[2]Department of Applied Science & Humanities, Sardar Vallabhbhai Patel Institute of Technology, Vasad, Gujarat - 388306, India

Abstract. The present study revisits the profound legacy of medicinal autotrophs, recognizing their historical significance in human healthcare and emphasizing the enduring collaboration between nature and humanity in the pursuit of therapeutic remedies. The research centers on biomolecules derived from natural autotrophs, namely Lupeol, Hederagenin, Quinovic acid, and Morolic acid, investigating their properties through a comprehensive computational analysis. Commencing with an emphasis on the historical context of medicinal plant usage, exemplified by Castanopsis indica and Anthocephalus cadamba in our country, the study highlights the diverse medicinal applications of plant-derived biomolecules. The computational analysis, utilizing density functional theory implemented by the Gaussian 09 package, reveals a fundamental understanding of Lupeol, Hederagenin, Quinovic acid, and Morolic acid. Molecular Electrostatic Potential (MESP) surfaces unveil potential sites for electrophilic and nucleophilic reactions, critical for drug-receptor interactions. . They have been found to be showing the strong characteristics of the commercially viable drugs as they exhibit values of Ionization potential and Electron affinity in the standard ranges as per FDA approved parameters. Further the findings associated with study of solvent effect on these biomolecules is helpful in exploring their molecular behaviour wherein Quinovic Acid showing the high dissolving nature in water medium (Solvation Energy 0.57 eV).The combined nature reveals their potential pharmacological applications in advanced drug research and development.

1. INTRODUCTION

As old as humanity itself, medicinal autotrophs have been used for mending health. There is substantial proof that humans and their hunt for remedies in nature have a long history together; which includes written records, preserved monuments, and even the original plant

* Corresponding author: prafullaj@yahoo.com

medicines [1]. The knowledge of using therapeutic plants came about as a result of person's long-standing battles with disease, which taught us to look for medicines in the barks, seeds, fruit bodies, and other parts of plants. Modern medicine already includes a variety of plant-based medications that have been around for millennia and were employed by ancient civilizations [2]. The ability of physicians and pharmacists to respond to challenges that have emerged with the spread of professional services in the facilitation of person's life has grown thanks to the expanding knowledge of the development of ideas pertaining to the usage of medicinal plants. In our country, plants such as Castanopsis indica and Anthocephalus cadamba have been identified for their biological accomplishment and depiction of the naturally occurring biomolecules [3][4].

There are several plant-derived biomolecules that have been explored for their medicinal applications by researchers. For example, Lupeol ($C_{30}H_{50}O$) is an important biomolecule found in Tamarind trees (Tamarindus indica), Varuna plants (Crateva nurvala), cotton trees (Bombax ceiba) [5][6], and Cadamba trees (Anthocephalus cadamba) [7]. A review article by Chaturvedi et al. suggests the chemo-preventive prospects of Lupeol [8]. It is an anti-inflammatory, anti-tumor, anti-microbial triterpene that can be pivotal in lowering cholesterol[9][10]. There are articles that discuss Lupeol's pharmacological properties, including significant anti-inflammatory and anti-diabetic potential, as demonstrated in studies involving Crateva adansonii[11]. Lupeol showed notable enzyme inhibition related to inflammation (e.g., COX-2 and myeloperoxidase) and diabetes (alpha-amylase and alpha-glucosidase). Additionally, Lupeol was investigated for its antiangiogenic activity in drug delivery systems aimed at treating ocular diseases like diabetic retinopathy, showing potential comparable to approved treatments. Finally, the compound was shown to inhibit tumor promotion induced by benzoyl peroxide in murine skin, suggesting its role as a chemopreventive agent. A computational study by Bodrikov et al. investigates an allylic bromination reaction mechanism of Lupeol[9]. Experimental studies have found it to be effectively working as a therapeutic agent for multiple pathogenic factors of acne. It has been successfully shown to be an effective skin cancer inhibitor[12].

Hederagenin ($C_{30}H_{48}O_4$) is a triterpenoid, which was first found in an English Ivy (Hedera helix) in the year 1849[13]. According to a comprehensive review article by Zeng et al, it exhibits anti-tumor, anti-inflammatory, anti-depressant, anti-neurodegenerative, anti-diabetic, and anti-viral (preventing from hepatitis B) properties[14]. With respect to the cancer treatment associated research in some of the promising studies it is investigated that Hedregenin induces apoptosis in Cisplatin –resistant Head and Cancer cells by inhibiting the Nrtz-ARE[15].Another advanced studies on this bio-molecule with respect to their experimental characteristics have revealed that it can evoke hemolysis on the erythrocytes, and has cytotoxic on various tumor cell lines,P-388,L-1210,U-937,NL-60,SNO-5 and HepG2[16]. Another study finding suggested that Hedregenin might be a promising therapeutic candidate for colon cancer[17].

Quinovic acid ($C_{30}H_{46}O_5$) is a notable biomolecule derived from South American Cat's claw vines (Uncaria tomentosa) and Indian cadamba trees, recognized for its diverse pharmacological properties[18]. As a glycoside, it has been found useful in treating hemorrhagic cystitis, a condition marked by inflammation and bleeding of the bladder lining. Additionally, Quinovic acid has shown promising anti-leishmanial activity, targeting parasites associated with black fever, making it a potential treatment for leishmaniasis[19].. In the realm of cancer therapy, it has been investigated for its role as an inhibitor in ferroptosis, a unique form of regulated cell death, suggesting its application in novel cancer treatments[20]. Furthermore, its cholesterol-resistive properties, as explored in recent studies, indicate potential benefits in managing dyslipidemia and reducing cardiovascular disease risk[21]. Notably, Quinovic acid's antiviral potential has also been highlighted, with recent

computational studies suggesting it might inhibit the main protease of SARS-CoV-2, the virus responsible for COVID-19. These diverse activities underscore Quinovic acid's potential as a valuable compound in the development of various therapeutic agents[22].
Another effective medicinal properties carrying biomolecule is Morolic acid ($C_{30}H_{48}O_3$), which is another triterpenoid, derived from Mora excelsa plants that are found in the woods of Caribbean islands [23][24]. It exhibits anti-hyperglycemic and anti-diabetic actions as per the work by Ramirez-Espinosa et al [25]. In the studies conducted by Zhang et al [29] it is found to be a naturally occurring pentcyclic triterpene whose derivatives exhibit promising ant HIV and other biological activities, it also exhibits inhibitory activity against glycogen phosphoylase (Tetrahedron) [26]. In another studies conducted by Kirstein et al revealed that Morolic Acid can inhibit leukotriene B4 production in rat polymorphonuclear leukvegtes stimulated with calcium ionosphere A23187 (Pharmacol Toxicol)[27][28].
Literature survey unveils the various applications of computational chemistry in drug discovery, with a particular focus on virtual screening, de novo design, the assessment of drug-likeness, and the exploration of advanced methods using computational approaches[29]. Therefore in this work, we have performed a computational investigation of the biomolecules Lupeol ($C_{30}H_{50}O$), Hederagenin ($C_{30}H_{48}O_4$), Quinovic acid ($C_{30}H_{46}O_5$), and Morolic acid ($C_{30}H_{48}O_3$). The reason behind the selection of said molecules is that all of these have same number (30) of carbon atoms. We have studied electronic properties such as density of states (DOS), energies of highest occupied molecular orbital (HOMO) and lowest unoccupied molecular orbital (LUMO), Fermi level, HOMO-LUMO energy gap, and dipole moment; reactivity parameters such as ionization potential, electrophilicity, chemical hardness, softness, and chemical potential. Apart from this, we have also obtained an IR spectrum for each biomolecule. We have also performed Frontal Molecular Analysis (FMO) and have undertaken the respective studies. To our best knowledge, the computational study for electronic and reactivity parameters for the above-mentioned biomolecules is yet to be performed. Our aim is to investigate the structural, electronic, and reactivity parameters of above-mentioned biomolecules in order to explore their further applications in the modern medicine.

2. COMPUTATIONAL DETAILS

The structure of the biomolecules (Lupeol, Morolic Acid, Quinovic Acid, Hedregenin) are optimized by using DFT calculations, which implemented by the Gaussian 09 package[30] with the application of B3LYP/6-31G level theory[31][32], as it correctly reproduces the molecular structures. The same level of theory was applied to compute total energies, electronic parameters, molecular orbitals (MO), and IR spectra. The visualization of structural geometry was performed using GaussView (version 6)[33], based on the results of DFT calculations. Density of states (DOS) plots were generated using the GaussSum tool[34]. Throughout the calculations, convergence criteria were maintained at 12×10^{-4} radians, 18×10^{-4} Bohr, 3×10^{-4} Hartree/radian, and 45×10^{-5} Hartree/Bohr for gradients of root-mean-square (rms) displacement, maximum displacement, rms force, and maximum force, respectively.
The electronic band gap and Fermi level energy were calculated from the following relations[35][36]:

$$E_g = E_{HOMO} - E_{LUMO} \text{ ---- (1)}$$

$$E_F = (E_{HOMO} - E_{LUMO})/2 \text{ ---- (2)}$$

Quantum chemical descriptors such as chemical potential (μ), softness (S), hardness (η), and electrophilicity (ω) are employed to evaluate the reactivity of biomolecules. These descriptors are determined by the equations provided below[37]:

$$\text{Chemical potential } (\mu) = -\frac{I+A}{2} \text{ --- (3)}$$

$$\text{Hardness } (\eta) = \frac{I-A}{2} \text{ --- (4)}$$

$$\text{Softness } (S) = \frac{1}{2\eta} \text{ --- (5)}$$

$$\text{Electrophilicity } (\omega) = \frac{\mu^2}{2\eta} \text{ --- (6)}$$

3. RESULTS AND DISCUSSION

3.1. Structural and Electronic Properties

First and foremost, the geometry optimization of the biomolecules Lupeol ($C_{30}H_{50}O$), Hederagenin ($C_{30}H_{48}O_4$), Quinovic acid ($C_{30}H_{46}O_5$), and Morolic acid ($C_{30}H_{48}O_3$) was performed. These biomolecules, consisting of carbon, hydrogen, and oxygen atoms, each contain a total of 30 carbon atoms. The optimization results for all four biomolecules are depicted in Fig. 1. Our computational findings closely match those reported in existing studies[9][38][16][39], affirming the reliability of our computational method. The optimized geometries offer valuable insights into the molecular structures of these compounds, revealing details about bond lengths, angles, and overall conformations. Furthermore, to validate the structural stability of these biomolecules, we conducted calculations to obtain their infrared (IR) spectra, as shown in Fig. 2. This step is crucial, especially considering that these molecules occur naturally.

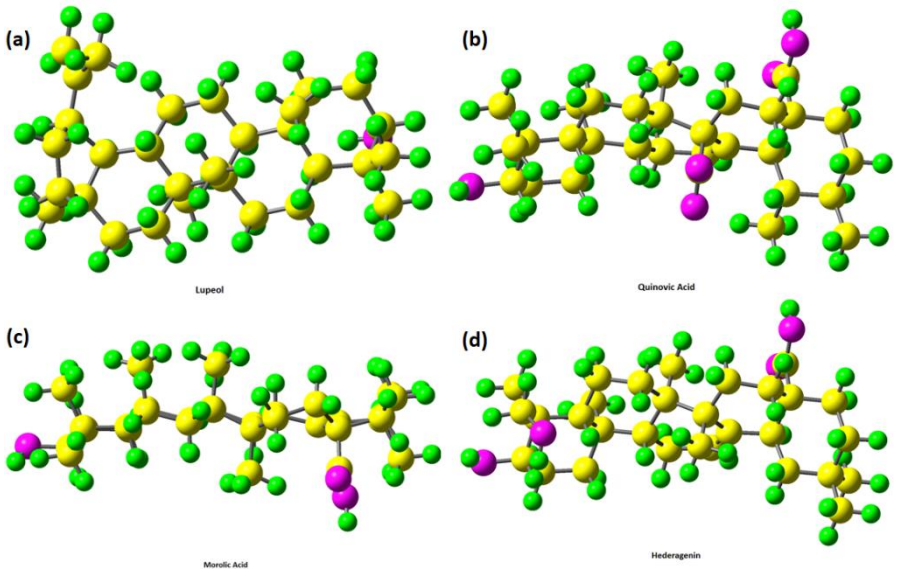

Fig. 1: Optimized molecular structures for (a) Lupeol, (b), Quinovic acid, (c) Morolic acid, and (d) Hederagenin

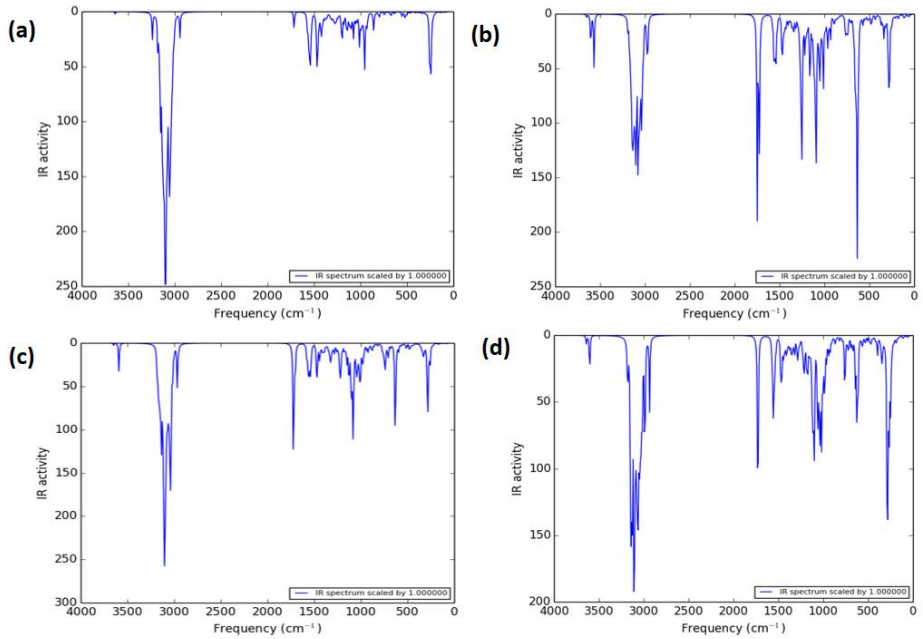

Fig. 2. IR spectra for (a) Lupeol, (b), Quinovic acid, (c) Morolic acid, and (d) Hederagenin

In terms of electronic properties, we have conducted calculations for the energies of the highest occupied molecular orbital (HOMO) and lowest unoccupied molecular orbital (LUMO), as well as the HOMO-LUMO energy gap (E_G), Fermi level (E_F), and molecular orbital spectra, also known as density of states (DOS) plots. The values of HOMO-LUMO energies, energy gaps, Fermi level can be seen in Table 1. For Lupeol, the HOMO energy is -6.29 eV, the LUMO energy is 0.59 eV, resulting in an E_G of 6.88 eV, with the Fermi level at -3.44 eV. Quinovic acid exhibits a HOMO energy of -6.1 eV, a LUMO energy of -0.56 eV, yielding an E_G of 6.05 eV, with the Fermi level at -3.58 eV. Morolic acid displays a HOMO energy of -6.16 eV, a LUMO energy of -0.26 eV, resulting in an E_G of 5.9 eV, with the Fermi level at -3.21 eV. Lastly, Hederagenin shows a HOMO energy of -5.99 eV, a LUMO energy of -5.99 eV, leading to an E_G of 5.78 eV, with the Fermi level at -3.1 eV. These electronic properties are corroborated by the molecular orbital spectra (DOS) illustrated in Fig. 3. Notably, the wide band gap (E_G > 5 eV) observed for all molecules suggests their potential classification as insulators. The frontier molecular orbital (FMO) diagrams along with their importance in the reactivity[40], are discussed in the supporting information section 1. Apart from the IR spectra the NMR and GC-MS experimental spectra are discussed in the supporting information section 2.

Table 1: Values of HOMO-LUMO energies, energy gaps, Fermi level

Biomolecule	**E_{HOMO} (eV)**	**E_{LUMO} (eV)**	**E_G (eV)**	**E_F(eV)**
Lupeol	6.29	-0.59	3.44	3.44
Quinovic acid	6.61	0.56	3.58	3.02
Morolic acid	6.16	0.26	3.21	2.95
Hederagenin	5.99	0.21	3.10	2.89

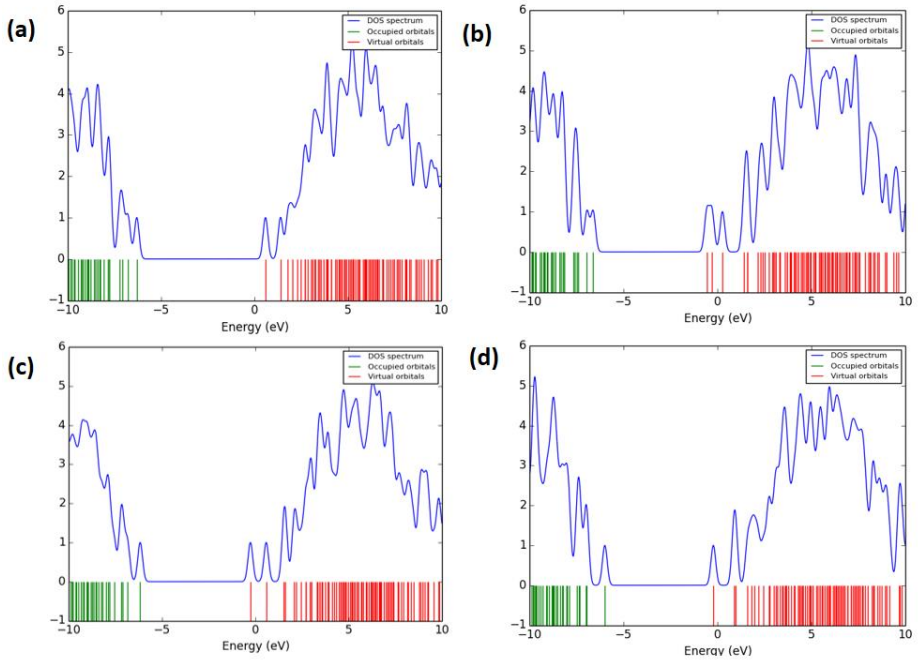

Fig. 3: Molecular orbital (DOS) spectra for (a) Lupeol, (b), Quinovic acid, (c) Morolic acid, and (d) Hederagenin

3.2. Molecular Electrostatic Potential (MESP) Analysis

The molecular electrostatic potential (MESP) maps provide valuable insights into the distribution of electron density within a molecule, allowing us to identify active or binding sites based on their electrostatic surface properties[41]. Each molecule exhibits distinct patterns in its MESP map, indicative of its unique electrostatic properties and potential binding sites. In these maps, red indicates electronegative regions, blue signifies positive regions, and green represents neutral regions. The maps presented in Fig. 4 offer valuable insights into the distribution of electron density within the biomolecules Lupeol, Hederagenin, Quinovic acid, and Morolic acid. Each molecule exhibits distinct patterns in its MESP map, indicative of its unique electrostatic properties and potential binding sites. In Lupeol, the most electronegative region is situated near the oxygen atom, underscoring its role in potential binding interactions due to its high electronegativity. Similarly, Hederagenin displays an electronegative region near the oxygen atom, suggesting its involvement in binding interactions, while an additional site near an O-H bond exhibits an electropositive region, indicating a more complex electrostatic environment. Quinovic acid reveals a negative region near a C-H bond and an electropositive region near the O-H bond, reflecting the polarity of different functional groups within the molecule. In Morolic acid, electropositive regions near the O-H bond signify potential binding sites, influencing the reactivity and binding affinity of a molecule. Overall, the MESP maps provide valuable information for identifying active sites and understanding the electrostatic properties of these biomolecules, essential for drug discovery and design applications.

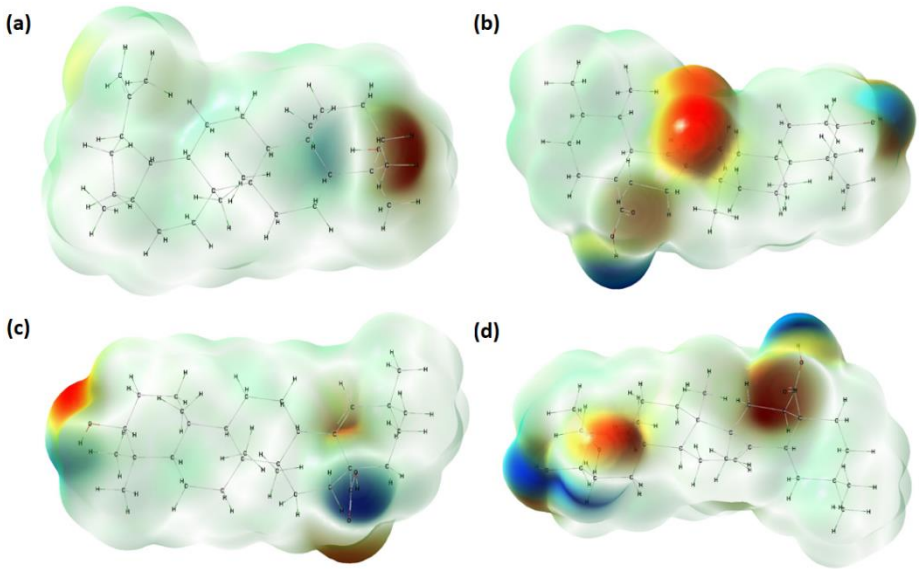

Fig. 4. MESP maps for (a) Lupeol, (b), Quinovic acid, (c) Morolic acid, and (d) Hederagenin

3.3. Frontier Molecular Orbitals

Frontier molecular orbitals (FMOs) are crucial in understanding chemical reactivity and bonding. The concept, introduced by Kenichi Fukui, focuses on the interactions between the highest occupied molecular orbital (HOMO) and the lowest unoccupied molecular orbital (LUMO) of reacting species. These orbitals are termed "frontier" because they lie at the boundary between occupied and unoccupied molecular orbitals. The HOMO represents the highest energy level that contains electrons, while the LUMO is the lowest energy level that can accept electrons. The interaction between these orbitals can predict the course of chemical reactions, as the HOMO of one molecule interacts with the LUMO of another, facilitating electron transfer and bond formation. This theory simplifies the prediction of reactivity and helps in understanding various chemical processes, including pericyclic reactions and acid-base interactions [40]. Figure 5 shows the FMO diagrams for Lupeol, Quinovic acid, Morolic acid, and Hederagenin.

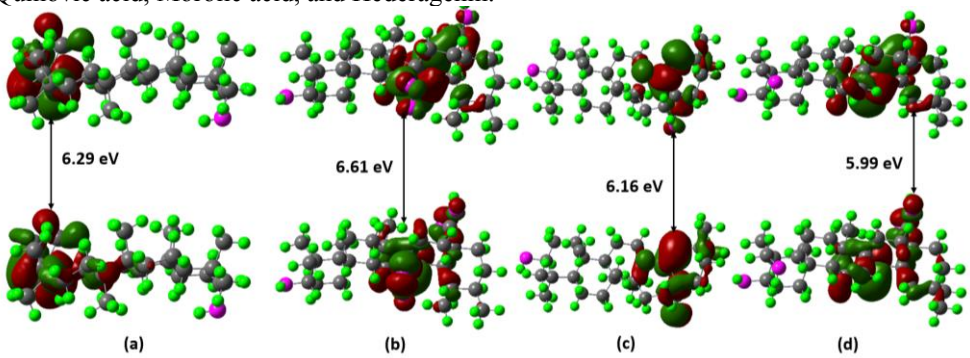

Fig. 5. FMO diagrams for (a) Lupeol, (b), Quinovic acid, (c) Morolic acid, and (d) Hederagenin

The highest occupied molecular orbital (HOMO) and lowest unoccupied molecular orbital (LUMO) plots of the biomolecules in the form of FMO diagrams is shown in Fig. 5. The frontier molecular orbital gap helps to characterize the chemical reactivity and kinetic stability of the molecule. The energy gap between HOMO and LUMO indicates the molecular chemical stability. The red color indicates the negative charge and green color indicates positive charge for the title molecule. The HOMO is orbital that indicates as an electron donor and the LUMO is the orbital that indicates as an electron acceptor. The Homo and LUMO values indicates the charge density localized places in and around the biomolecules. The calculated HOMO and LUMO energies as given in Table 1 clearly shows that charge transfer occurs within the molecule. The calculated HOMO-LUMO energy gap value is found to be 6.29 eV,6.61 eV,6.16 eV and 5.99 eV respectively as shown in Figure 5.

3.4. Reduced Density Gradient (RDG) Plots

We utilized the *Multiwfn* software[42] to generate plots of the reduced density gradients (RDG). The RDG plots serve as a valuable analytical tool for elucidating the attractive and repulsive aspects of interatomic interactions within molecules, as well as for assessing and characterizing the strength of these interactions. Positive λ_2 values reveal strong attractive forces within the charge density, while negative λ_2 values indicate repulsive forces. When $\rho = 0$, the plots correspond to van der Waals forces[43]. Fig. 6 shows the RDG plots for Lupeol, Quinovic acid, Morolic acid, and Hederagenin.

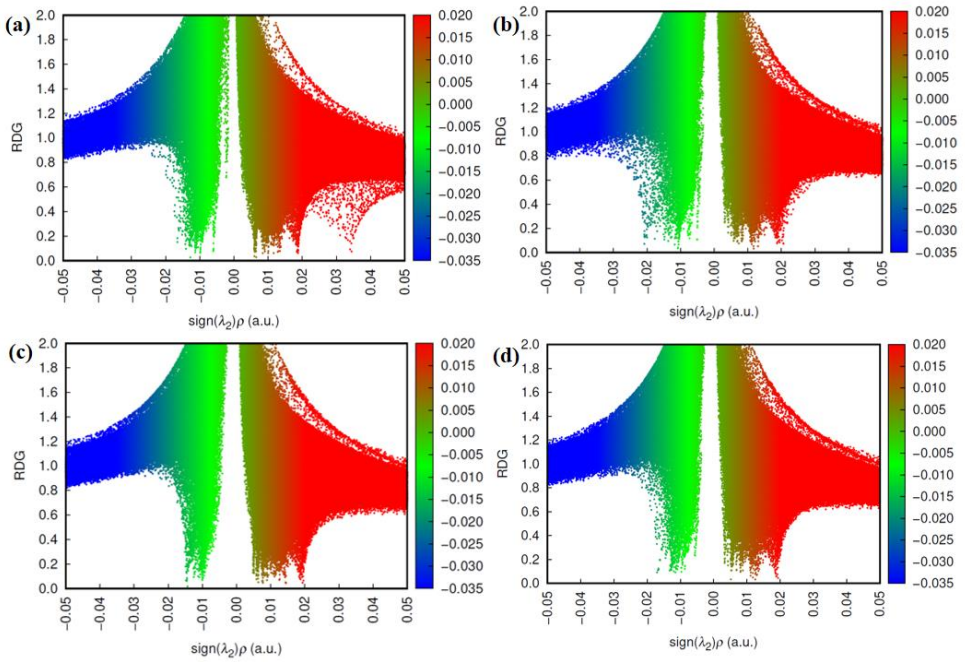

Fig. 6. RDG plots for (a) Lupeol, (b), Quinovic acid, (c) Morolic acid, and (d) Hederagenin

3.5. Reactivity Parameters

According to Koopman's theorem[44], the highest occupied molecular orbital (HOMO) and lowest unoccupied molecular orbital (LUMO) serve as effective approximations for the negative ionization potential (E_{HOMO} = -I) and negative electron affinity (E_{LUMO} = -A),

respectively. Quantum chemical descriptors such as chemical potential (μ), softness (S), hardness (η), and electrophilicity (ω) are employed to evaluate the reactivity of biomolecules.

Table 2: Ionization potential (I), electron affinity (A), chemical potential (μ), hardness(η), softness (S), and electrophilicity (ω)

Biomolecule	**I (eV)**	**A (eV)**	**μ (eV)**	**η (eV)**	**S (eV^{-1})**	**ω (eV)**
Lupeol	6.29	-0.59	3.44	3.44	0.145	1.72
Quinovic acid	6.61	0.56	3.58	3.02	0.165	2.12
Morolic acid	6.16	0.26	3.21	2.95	0.169	1.75
Hederagenin	5.99	0.21	3.10	2.89	0.173	1.66

Table 2 provides the ionization potential and electron affinity values for the biomolecules, along with other quantum chemical descriptors calculated using the aforementioned equations. Fig. 7 graphically presents the comparison of ionization potential and other quantum chemical descriptors.

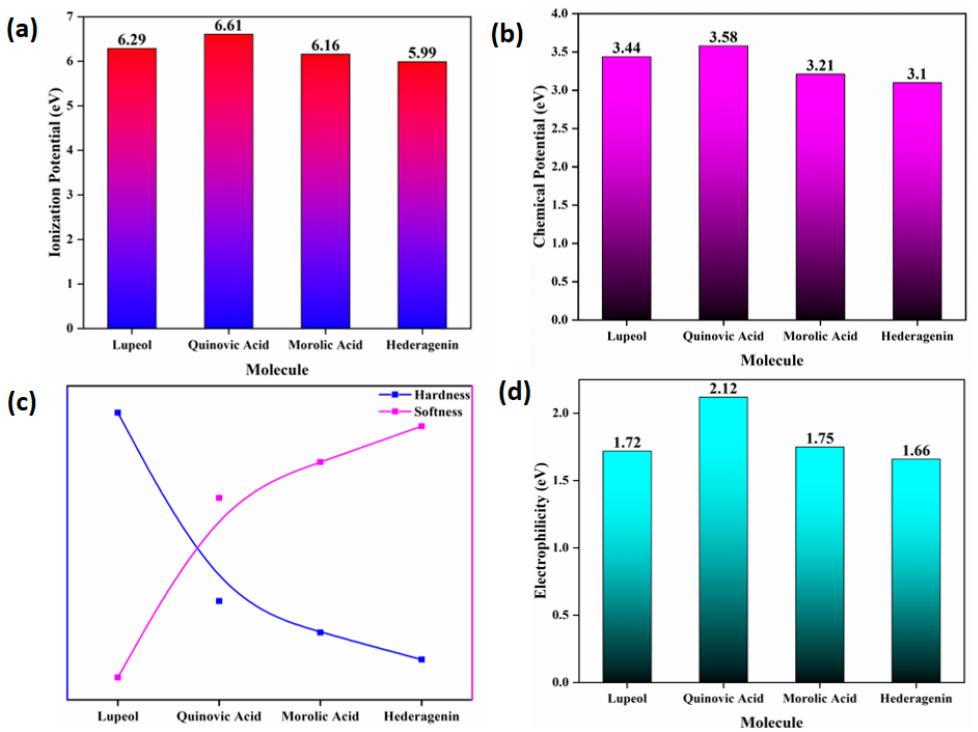

Fig. 7. Graphical representation of the comparison of ionization potential and other quantum chemical descriptors.

The prevailing belief suggests that a higher ionization potential correlates with lower toxicity [45]. The ionization potential order follows Quinovic acid > Lupeol > Morolic acid > Hederagenin. Electron affinity (A) is highest for Quinovic acid, but for Lupeol, it is negative. Considering that chemical potential (μ) correlates with reactivity and likely drug efficacy[46], the μ order aligns with Quinovic acid > Lupeol > Morolic acid > Hederagenin. Among these molecules, Lupeol exhibits the highest chemical hardness, while Hederagenin demonstrates the lowest. Conversely, chemical softness shows the opposite trend, with

Lupeol having the lowest softness and Hederagenin displaying the highest, as depicted in Fig. 7(c). Additionally, electrophilicity (ω) is observed to be highest for Quinovic acid and lowest for Hederagenin. These findings provide valuable insights into the reactivity and potential efficacy of these anticancer drugs.
The values of the Ionization potential (IP) signifies the easiness for an electron donation of a compound and the Electron affinity (EA) represents easiness for accepting electron. The electron obstruction is one of the mechanisms for toxicity by redox property. The redox instability or toxicity increases with decrease in Ionization Potential (IP) and increase in Electron affinity (EA) values. Further the stable FDA approved or commercialized drugs usually exhibit standard values for the Ionization potential and Electron affinity in the ranges of 4 eV to 15 eV and less than -10 eV respectively[47]. On comparing their values from the table 2 above they have been found to be more suitable to be used as commercially viable drug molecules[48].

3.6. Solvent Effect

In this study, we have also considered the solvent effect, which was calculated using the Integral Equation Formalism Polarizable Continuum Model (IEFPCM) method[49]. Specifically, we investigated the influence of water solvent through the calculation of solvation energy. Solvation energy is defined as the difference between the ground state energy of the biomolecule in a gaseous medium and in a water medium[50][51].

$$E_{solvation} = E_{gaseous} - E_{water} \text{ ---- } (7)$$

Table 3: Ground state energies of biomolecules in both gaseous and water mediums, with solvation energies.

Biomolecule	Ground state energy (hartree)		Solvation energy (eV)
	In gaseous medium	In water	
Lupeol	-1248.185627	-1248.192576	0.19
Quinovic acid	-1546.595201	-1546.616101	0.57
Morolic acid	-1397.382969	-1397.396368	0.22
Hederagenin	-1472.580878	-1472.599669	0.51

In the case of Lupeol, the solvation energy was determined to be 0.19 eV, while for Quinovic acid, it was found to be 0.57 eV. Similarly, Morolic acid exhibited a solvation energy of 0.22 eV, and Hederagenin displayed a solvation energy of 0.51 eV. These values provide insights into the interaction between the biomolecules and water solvent, offering valuable information for understanding their behavior in biological environments. Higher solvation energy indicates strong interactions between a molecule and the surrounding solvent[52], in this case, water. This implies that, Quinovic acid dissolves best in water medium. The data presenting ground state energies in both gaseous and water mediums, alongside solvation energies, is organized in Table 3.

4. CONCLUSION

Our study explores essential electronic properties and reactivity patterns within the biomolecules Lupeol, Quinovic acid, Morolic acid, and Hederagenin. Through Density Functional Theory (DFT) simulations, we understood distinct variations in ionization potential, chemical potential, chemical hardness, softness, and electrophilicity among these

compounds. Lupeol stands out for its notable reactivity features, characterized by heightened chemical hardness and reduced softness, suggesting potential stability and interaction possibilities. Quinovic acid exhibits high electrophilicity, indicating a preference for electron transfer activities. Morolic acid demonstrates intermediate reactivity, whereas Hederagenin displays lower chemical potential and electrophilicity, indicating weaker contact potentials. Moreover, our analysis reveals the solvent effect, with Quinovic acid displaying enhanced solubility in water. These findings provide valuable insights into the molecular behavior and potential pharmacological applications of these biomolecules in drug research and development.

References

1. B.B. Petrovska, Historical review of medicinal plants' usage, Pharmacogn. Rev. 6 (2012) 1–5. https://doi.org/10.4103/0973-7847.95849.
2. J. Sendker, H. Sheridan, History and current status of herbal medicines, Toxicol. Herb. Prod. (2017) 11–27. https://doi.org/10.1007/978-3-319-43806-1_2.
3. N. Dolai, I. Karmakar, R.B.S. Kumar, B. Kar, A. Bala, P.K. Haldar, Free radical scavenging activity of Castanopsis indica in mediating hepatoprotective activity of carbon tetrachloride intoxicated rats, Asian Pac. J. Trop. Biomed. 2 (2012) 24–26. https://doi.org/10.1016/S2221-1691(12)60168-3.
4. A. Dubey, S. Nayak, D.C. Goupale, Anthocephalus cadamba: A review, Pharmacogn. J. 2 (2011) 71–76. https://doi.org/10.1016/S0975-3575(11)80029-5.
5. M. Saleem, Lupeol, a novel anti-inflammatory and anti-cancer dietary triterpene, Cancer Lett. 285 (2009) 109–115. https://doi.org/10.1016/j.canlet.2009.04.033.
6. H.R. Siddique, M. Saleem, Beneficial health effects of lupeol triterpene: A review of preclinical studies, Life Sci. 88 (2011) 285–293. https://doi.org/10.1016/j.lfs.2010.11.020.
7. A. Wal, R.. Srivastava, P. Wal, A. Rai, S. Sharma, Lupeol as a magical drug, Pharm. Biol. Eval. 2 (2015) 142–151.
8. P.K. Chaturvedi, K. Bhui, Y. Shukla, Lupeol: Connotations for chemoprevention, Cancer Lett. 263 (2008) 1–13. https://doi.org/10.1016/j.canlet.2008.01.047.
9. I. V. Bodrikov, Y.A. Kurskii, A.A. Chiyanov, A.Y. Subbotin, Selenium Dibromide as a Reagent for Selective Allylic Bromination of Diacetylbetulin and Lupeol, Russ. J. Org. Chem. 58 (2022) 1178–1179. https://doi.org/10.1134/S1070428022080140.
10. M. Saleem, F. Afaq, V.M. Adhami, H. Mukhtar, Lupeol modulates NF-, (2004) 1–11.
11. T. Rathinavel, M.N. Iqbal, S. Kumarasamy, Lupeol from Crateva adansonii DC Exhibits Promising Enzymes Inhibition: Play a Crucial Role in Inflammation and Diabetes, South African J. Bot. 143 (2021) 449–456. https://doi.org/10.1016/j.sajb.2021.08.023.
12. M. Saleem, A. Alam, S. Arifin, M.S. Shah, B. Ahmed, S. Sultana, Lupeol, a triterpene, inhibits early responses of tumor promotion induced by benzoyl peroxide in murine skin, Pharmacol. Res. 43 (2001) 127–134. https://doi.org/10.1006/phrs.2000.0710.
13. M. Yu, Y.J. Shin, N. Kim, G. Yoo, S.J. Park, S.H. Kim, Determination of Saponins and Flavonoids in Ivy leaf extracts using HPLC-DAD, J. Chromatogr. Sci. 53 (2015) 478–483. https://doi.org/10.1093/chromsci/bmu068.
14. J. Zeng, T. Huang, M. Xue, J. Chen, L. Feng, R. Du, Y. Feng, Current knowledge and development of hederagenin as a promising medicinal agent: A comprehensive review, RSC Adv. 8 (2018) 24188–24202. https://doi.org/10.1039/c8ra03666g.

15. K. Wang, X. Liu, Q. Liu, I. ht Ho, X. Wei, T. Yin, Y. Zhan, W. Zhang, W. Zhang, B. Chen, J. Gu, Y. Tan, L. Zhang, M.T. Chan, W.K. Wu, B. Du, J. Xiao, Hederagenin potentiated cisplatin- and paclitaxel-mediated cytotoxicity by impairing autophagy in lung cancer cells, Cell Death Dis. 11 (2020). https://doi.org/10.1038/s41419-020-02880-5.
16. M. Yang, J. Wang, Q. Wang, Hederagenin Exerts Potential Antilipemic Effect via p38MAPK Pathway in Oleic Acid-induced HepG2 cells and in Hyperlipidemic Rats, An. Acad. Bras. Cienc. 94 (2022) 1–11. https://doi.org/10.1590/0001-3765202220201909.
17. B.X.Z. Liu, J.Y. Zhou, Y. Li, X. Zou, J. Wu, J.F. Gu, J.R. Yuan, B.J. Zhao, L. Feng, X. Bin Jia, R.P. Wang, Hederagenin from the leaves of ivy (Hedera helix L.) induces apoptosis in human LoVo colon cells through the mitochondrial pathway, BMC Complement. Altern. Med. 14 (2014) 412. https://doi.org/10.1186/1472-6882-14-412.
18. F. Dietrich, J.P. Martins, S. Kaiser, R.B.M. Silva, L. Rockenbach, M.I.A. Edelweiss, G.G. Ortega, F.B. Morrone, M.M. Campos, A.M.O. Battastini, The quinovic acid glycosides purified fraction from uncaria tomentosa protects against hemorrhagic cystitis induced by cyclophosphamide in mice, PLoS One. 10 (2015) 1–15. https://doi.org/10.1371/journal.pone.0131882.
19. C. Di Giorgio, M. Lamidi, F. Delmas, G. Balansard, E. Ollivier, Antileishmanial activity of quinovic acid glycosides and cadambine acid isolated from Nauclea diderrichii, Planta Med. 72 (2006) 1396–1402. https://doi.org/10.1055/s-2006-951726.
20. X. Liang, Y. Wei, X. Hou, Q. Guo, H. Liang, K. Zeng, P. Tu, Q. Zhang, Triterpenoids from Uncaria macrophylla as ferroptosis inhibitors, Phytochemistry. 206 (2023) 11–12. https://doi.org/10.1016/j.phytochem.2022.113530.
21. K. Saeed, S.A. Shah, R. Ullah, S.I. Alam, J.S. Park, S. Saleem, M.H. Jo, M.W. Kim, J.R. Hahm, M.O. Kim, Quinovic Acid Impedes Cholesterol Dyshomeostasis, Oxidative Stress, and Neurodegeneration in an Amyloid- β -Induced Mouse Model, Oxid. Med. Cell. Longev. 2020 (2020). https://doi.org/10.1155/2020/9523758.
22. A.F. Yepes-Pérez, O. Herrera-Calderon, J.E. Sánchez-Aparicio, L. Tiessler-Sala, J.D. Maréchal, W. Cardona-G, Investigating Potential Inhibitory Effect of Uncaria tomentosa (Cat's Claw) against the Main Protease 3CLproof SARS-CoV-2 by Molecular Modeling, Evidence-Based Complement. Altern. Med. 2020 (2020). https://doi.org/10.1155/2020/4932572.
23. T.P. I, B.D.H.R. Barton, 257 60., (1951) 257–277.
24. M. Acid, A.T. Sapogenin, Communications To T H E , E D I T O R, 72 (1946) 3314.
25. J.J. Ramírez-Espinosa, S. García-Jiménez, M.Y. Rios, J.L. Medina-Franco, F. López-Vallejo, S.P. Webster, M. Binnie, M. Ibarra-Barajas, R. Ortiz-Andrade, S. Estrada-Soto, Antihyperglycemic and sub-chronic antidiabetic actions of morolic and moronic acids, in vitro and in silico inhibition of 11β-HSD 1, Phytomedicine. 20 (2013) 571–576. https://doi.org/10.1016/j.phymed.2013.01.013.
26. Y. Kashiwada, H.-K. Wang, T. Nagao, S. Kitanaka, I. Yasuda, T. ve ark Fujioka, Anti-AIDS Agents . 30 . Anti-HIV Activity of Oleanolic Acid , Pomolic Acid , and, J. Nat. Prod. 61 (1998) 1090–1095.
27. Bernardi MM, Spinosa HS, Ricci EL, Reis-Silva TM, Anti-nociceptive and anti-inflammatory actions of Nepeta cataria L. var. citriodora (Becker) Balb. essential oil in mice, Rev. Do Inst. Ciências Da Saúde. 28 (2010) 289–293.
28. Y. Huang, J. Li, R. Wang, Q. Wu, Y.H. Li, S.C. Yu, W.M. Cheng, Y.Y. Wang, Effect of triterpene acids of Eriobotrya japonica (thunb.) lindl. leaf on inflammatory cytokine and mediator induction from alveolar macrophages of chronic bronchitic rats, Inflamm. Res. 56 (2007) 76–82. https://doi.org/10.1007/s00011-006-5185-0.

29. W.L. Jorgensen, The Many Roles of Computation in Drug Discovery, Science (80). 303 (2004) 1813–1818. https://doi.org/10.1126/science.1096361.
30. et al. M. J. Frisch, Trucks, G.W., Schlegel, H.B., Scuseria, G.E., Robb, M.A., Cheeseman, J.R., Gaussian 09 Citation, Gaussian 09, Revis. A.02, Gaussian, Inc. (2016) 1–2. http://www.gaussian.com/g_tech/g_ur/m_citation.htm.
31. J. Tirado-Rives, W.L. Jorgensen, Performance of B3LYP density functional methods for a large set of organic molecules, J. Chem. Theory Comput. 4 (2008) 297–306. https://doi.org/10.1021/ct700248k.
32. J.E. Del Bene, D.H. Aue, I. Shavitt, 6-3 1 1, (1992) 1631–1640.
33. R. Dennington, T. Keith, J. Millam, GaussView, Version 6, Roy Dennington, Todd Keith, and John Millam, Semichem Inc., Shawnee Mission, KS, 2019., (2019) 2019.
34. N.M. O'Boyle, A.L. Tenderholt, K.M. Langner, Cclib: A library for package-independent computational chemistry algorithms, J. Comput. Chem. 29 (2008) 839–845. https://doi.org/10.1002/jcc.20823.
35. N.R. Sheela, S. Muthu, S. Sampathkrishnan, Molecular orbital studies (hardness, chemical potential and electrophilicity), vibrational investigation and theoretical NBO analysis of 4-4′-(1H-1,2,4-triazol-1-yl methylene) dibenzonitrile based on abinitio and DFT methods, Spectrochim. Acta - Part A Mol. Biomol. Spectrosc. 120 (2014) 237–251. https://doi.org/10.1016/j.saa.2013.10.007.
36. Y. Liu, C. Liu, A. Kumar, A selective NO sensor based on the semiconducting BC2N nanotubes: a computational study, Mol. Phys. 118 (2020) 1–8. https://doi.org/10.1080/00268976.2020.1798528.
37. S. Vadalkar, D. Chodvadiya, N.N. Som, K.N. Vyas, P.K. Jha, Cyclo18.carbon as a Hazardous Gas Scavenger: Effect of Boron and Nitrogen Doping on Molecular Adsorption, ChemistrySelect. 8 (2023) e202204862. https://doi.org/10.1002/slct.202204862.
38. R. Aquino, N. De Tommasi, F. De Simone, C. Pizza, Triterpenes and quinovic acid glycosides from Uncaria tomentosa, Phytochemistry. 45 (1997) 1035–1040. https://doi.org/10.1016/S0031-9422(96)00716-9.
39. A. Dwevedi, K. Sharma, Y.K. Sharma, Cadamba : A miraculous tree having enormous pharmacological implications, Pharmacogn. Rev. 9 (2015) 107–113. https://doi.org/10.4103/0973-7847.162110.
40. J. Yu, N.Q. Su, W. Yang, Describing Chemical Reactivity with Frontier Molecular Orbitalets, JACS Au. 2 (2022) 1383–1394. https://doi.org/10.1021/jacsau.2c00085.
41. B. Shivaleela, G.G. Shivraj, S.M. Hanagodimath, Estimation of dipole moments by Solvatochromic shift method, spectroscopic analysis of UV–Visible, HOMO-LUMO, ESP map, Mulliken atomic charges, NBO and NLO properties of benzofuran derivative, Results Chem. 6 (2023) 101046. https://doi.org/10.1016/j.rechem.2023.101046.
42. T. Lu, F. Chen, Multiwfn: A multifunctional wavefunction analyzer, J. Comput. Chem. 33 (2012) 580–592. https://doi.org/10.1002/jcc.22885.
43. N.A. Tukadiya, S.K. Jana, B. Chakraborty, P.K. Jha, C24 Fullerene and its derivatives as a viable glucose sensor: DFT and TD-DFT studies, Surfaces and Interfaces. 41 (2023) 1–16. https://doi.org/10.1016/j.surfin.2023.103220.
44. T. Tsuneda, J.W. Song, S. Suzuki, K. Hirao, On Koopmans' theorem in density functional theory, J. Chem. Phys. 133 (2010). https://doi.org/10.1063/1.3491272.
45. I.M.M. Othman, M.H. Mahross, M.A.M. Gad-Elkareem, M. Rudrapal, N. Gogoi, D. Chetia, K. Aouadi, M. Snoussi, A. Kadri, Toward a treatment of antibacterial and antifungal infections: Design, synthesis and in vitro activity of novel arylhydrazothiazolylsulfonamides analogues and their insight of DFT, docking and

molecular dynamic simulations, J. Mol. Struct. 1243 (2021) 1–5. https://doi.org/10.1016/j.molstruc.2021.130862.
46. K.S. Sakariassen, S.R. Hanson, Y. Cadroy, Methods and models to evaluate shear-dependent and surface reactivity-dependent antithrombotic efficacy, Thromb. Res. 104 (2001) 149–174. https://doi.org/10.1016/S0049-3848(01)00344-9.
47. Exploring the co-activity of FDA approved drug gemcitabine and docetaxel for enhanced anti-breast cancer activity_ DFT, docking, molecular dynamics simulation and pharmacophore studies - Sukumaran - 2024 - International Journal of Quantum Chemistry - .pdf, (n.d.).
48. P.S. Sen Gupta, H.R. Bhat, S. Biswal, M.K. Rana, Computer-aided discovery of bis-indole derivatives as multi-target drugs against cancer and bacterial infections: DFT, docking, virtual screening, and molecular dynamics studies, J. Mol. Liq. 320 (2020) 1–6. https://doi.org/10.1016/j.molliq.2020.114375.
49. A. Klamt, C. Moya, J. Palomar, A Comprehensive Comparison of the IEFPCM and SS(V)PE Continuum Solvation Methods with the COSMO Approach, J. Chem. Theory Comput. 11 (2015) 4220–4225. https://doi.org/10.1021/acs.jctc.5b00601.
50. S. Kanti Jana, N.N. Som, P.K. Jha, Theoretical appraisements on the interaction behaviour of amphetamine, ketamine and mercaptopurine drug molecules over C24 fullerene: A combined dispersion corrected DFT and MD simulation study, J. Mol. Liq. 383 (2023) 1–4. https://doi.org/10.1016/j.molliq.2023.122084.
51. A. Kanzariya, S. Vadalkar, L.K. Saini, P.K. Jha, Cyclo16.carbon through the lens of density functional theory: Role of impurity decoration in hydrogen evolution reaction, Int. J. Hydrogen Energy. 71 (2024) 400–410. https://doi.org/10.1016/j.ijhydene.2024.05.236.
52. M. Perveen, S. Nazir, A.W. Arshad, M.I. Khan, M. Shamim, K. Ayub, M.A. Khan, J. Iqbal, Therapeutic potential of graphitic carbon nitride as a drug delivery system for cisplatin (anticancer drug): A DFT approach, Biophys. Chem. 267 (2020) 106461. https://doi.org/10.1016/j.bpc.2020.106461.